Author

In her project, Yekaterina Pavlova applied nonlinear partial differential equations and numerical analysis to the problem of modeling shock formation, and her experience taught her how useful new mathematical techniques can be in simplifying difficult engineering problems. Yekaterina started graduate school at California Institute of Technology in Fall 2006, with an ultimate goal of being able to advance and revolutionize technology by applying new mathematical ideas to current problems. She quotes a favorite professor as saying, "It's a very dangerous thing to believe you understand something," and she credits her research experience with helping her learn to look beyond obvious answers to find more important questions.

Key Terms

- α-Regularization
- Burgers Equation
- Entropy Condition
- Finite Difference Schemes
- Leray-α
- Numerical Partial Differential Equations

Convergence of the Leray α-Regularization Scheme for Discontinuous Entropy Solutions of the Inviscid Burgers Equation

Yekaterina S. Pavlova
Aerospace Engineering & Mathematics

Abstract

In this paper we explore the use of the Leray α-regularization applied to the inviscid Burgers equation. In this regularization, an additional variable is introduced, which is a smoothed version of the original variable, and a vector system for the original and smoothed variable is solved simultaneously. We employ a hybrid algorithm combining a centered finite difference scheme for Burgers equation and a spectral method for the regularization. A parameter θ is introduced in order to conserve particular quantities associated with the solution of the regularized problem. For several values of θ, we compare the exact solutions to those of the regularized problem and investigate the dependence of the solutions on the regularization parameter α and on the mesh size. In particular, it is shown that under appropriate conditions and particular values of θ, the numerical Leray α-regularization scheme produces an approximate solution that appears to converge to the unique discontinuous (entropy) solution of Burgers equation as the mesh size $h \to 0$, provided that the regularization parameter α and h are related to each other in a precise way. Interestingly, our results suggest that it is only the smoothed variable that converges to the entropy solution.

Faculty Mentors

This research introduces a novel approach—inspired by recent developments in sub-grid scale models of turbulence—for computing hyperbolic conservation laws that arise in many problems including aircraft design, tsunami waves, and traffic bottlenecks. These equations are known to develop singularities in finite time, and capturing the physical solution beyond the singularity time has been a major challenge for the past half-century. Here, this novel approach is tested thoroughly using Burgers equation as a prototype, and the success and limitations of the approach are determined. Being involved in such state-of-the-art research provides undergraduates with a unique opportunity to bridge classroom mathematics experience and knowledge with real world applications.

John S. Lowengrub
School of Physical Sciences &
Henry Samueli School of Engineering

Edriss S. Titi
School of Physical Sciences &
Henry Samueli School of Engineering

Introduction

Many problems in engineering and science involve conserved quantities, and mathematical modeling of such problems leads to systems of conservation laws. Mass, momentum and energy conservation laws derived for various types of fluid flows together with equations of state form a sufficient set of governing equations. For example, shock waves in supersonic nozzle exhaust, tsunami waves, traffic bottlenecks, and numerous other phenomena can be modeled very successfully with conservation laws. Amazingly, the same forms of conservation laws are applicable to seemingly different physical processes; therefore an advance in the understanding of solutions of one equation contributes to several applied fields of study simultaneously.

This paper explores new numerical techniques for solving such conservation laws by focusing on a specific model problem: Burgers equation. Burgers equation is one of the simplest and most well studied nonlinear hyperbolic partial differential equations, as it serves as a model for more general conservation laws (Knobel, 2000). In fluid mechanics the Burgers equation is the special case of Newton's second law (momentum conservation), applied to a differential volume of inviscid compressible fluid with no pressure gradients and no external body forces. Such approximation is valid in most applications in aerodynamics because the inviscid theory is applicable outside any boundary layers (thin viscous flow regions surrounding the immersed body). Thus Burgers equation can be used to model compressible fluid flow far from a moving body. This particularly applies to shock wave formation in supersonic compressible flow—a phenomenon at the heart of the design consideration of any space launch vehicle.

The prime difficulty in computing conservation laws arises from nonlinearity of the governing equations. Not only may discontinuities develop in an initially smooth profile, in many cases more than one solution exists for the given problem. The concept of a weak solution has been introduced to deal with solution discontinuities that develop in finite time, since the solution in the classical sense (continuously differentiable) no longer exists in that case. A weak solution is obtained by considering a given conservation law in its integral form as opposed to the classical differential form, which with some manipulation allows the computation of solutions that are discontinuous and does not require differentiability to satisfy the posed problem. However, different equivalent forms of the same differential equation may produce different weak solutions, introducing non-uniqueness and of course greater difficulty in dealing with such problems.

Existence and uniqueness results are crucial preliminaries to any solution scheme of a particular problem. If the additional conditions required for uniqueness are not imposed in the solution procedure, there is no guarantee that the obtained result represents the desired physically meaningful solution. A great deal of theoretical work has been done to obtain necessary and sufficient conditions for the existence and uniqueness of solutions to conservation laws but in many cases, as for example the 3-D momentum conservation equation (viscous Navier-Stokes equations or inviscid Euler equations), we still do not have a uniqueness result that is valid for a general class of initial data.

Regularization schemes modify the existing equations and force the solutions of the regularized problem to be smooth rather than discontinuous. In the limit as the regularization parameter tends to zero, the regularized equation formally tends to the original equation. Further, it is often easier to simulate numerically the solution of the regularized equation than the original equation.

In this paper we study the convergence properties of a particular regularization scheme applied to Burgers equation. The solution is demonstrated numerically to converge to a unique physically meaningful result given a particular setup of the regularization problem. The new method is easy to implement numerically and gives a good degree of accuracy in relation to the exact solution, making it a promising candidate for use in computation in engineering applications.

Background

Burgers equation is a special case of a general conservation law:

$$u_t(x,t) + f(u(x,t))_x = 0 \qquad (1)$$

where $u(x,t)$ is the amount of a conserved quantity such as density, momentum or internal energy, $f(u)$ describes the flux of the conserved quantity, in the case of Burgers equation, $f(u) = \frac{1}{2}u^2$, and the subscripts denote partial derivatives. The inviscid form of Burgers equation that is to be considered here is given by:

$$u_t(x,t) + u(x,t)u_x(x,t) = 0 \qquad x \in \mathbb{R},\ t > 0 \qquad (2)$$

together with L-periodic (L = 1) initial conditions:

$$u(x,0) = \varphi(x) = \varphi(x + L) \qquad x \in \mathbb{R} \qquad (3)$$

Assuming that no discontinuities develop in time, the solution u(x,t) can be obtained by the method of characteristics in the same way as for the linear advection (wave) equation $u_t + cu_x = 0$, except here the characteristic speed is no longer constant (Knobel 135). The solution u(x,t) is constant along the characteristic curves which, for Burgers equation, are given by:

$$x(t) = \varphi(x_0)\, t + x_0 \tag{4}$$

The solution u(x,t) is then given by:

$$u(x,t) = \varphi(x_0(x,t)) \tag{5}$$

where x_o is a zero of the function:

$$0 = G(x_0) = x - \varphi(x_0)\, t - x_0 \tag{6}$$

(Strauss 361). If $\frac{d\varphi(x_o)}{dx_o} \geq 0$, this equation is uniquely solvable for all t. In this case, the solution is an expansion fan or is a constant in the case of equality. The characteristics do not intersect, so unless initial conditions are discontinuous, the solution u(x,t) will remain smooth for all times. However, if $\frac{d\varphi(x_o)}{dx_o} < 0$ for some x_o in the initial periodic profile then equation (6) may not be uniquely solvable for x_o, for all t. As a consequence some of the characteristics intersect, resulting in discontinuities (shocks) and non-differentiability of the solution. However, it is still possible to obtain the solution in the weak (or integral) sense (LeVeque 27). Such solutions typically are piecewise smooth. In the case of a single jump discontinuity, let $(x_s(t),t)$ be a curve in the x–t plane across which u(x,t) is discontinuous. Then the time variation of the curve is given by the Rankine-Hugoniot condition (Knobel 134):

$$\dot{x}_s(t) \equiv \frac{dx_s}{dt} = \frac{f(u^+) - f(u^-)}{u^+ - u^-} = \frac{1}{2}(u^+ + u^-) \tag{7}$$

The discontinuity in the solution is called a shock wave, $\dot{x}_s(t)$ is the speed of propagation, $u^+ = \lim_{x \to x_s^+} u(x,t)$ and $u^- = \lim_{x \to x_s^-} u(x,t)$ are right and left limits that will in general not be equal across the shock wave, creating an infinite spatial gradient of u(x,t). If the shock is not present initially, the time of formation is calculated as the smallest time when $u_x(x,t)$ becomes infinite, which is given by:

$$t_b = \inf\left\{ t > 0,\ t = \frac{-1}{(\partial\varphi(x_0)/\partial x_0)}\ \text{, for all } x_0 \in \mathbb{R} \right\} \tag{8}$$

Lastly, to ensure uniqueness of the weak solution, the entropy condition is used as the physical selection mechanism. That is, the speed of the wave just behind the shock must be higher than the speed just ahead of it (Strauss 366). The entropy condition guarantees (in analogy with gas dynamics) that the entropy of material increases as it passes through the discontinuity. This can be written as:

$$u^- > \dot{x}_s(t) > u^+ \tag{9}$$

for Burgers equation. Hence, the solution that satisfies the entropy condition is a unique physical solution. A more convenient method to test if the entropy condition is satisfied is the Oleinik inequality (Knobel 183):

$$\frac{u(x + a,t) - u(x,t)}{a} < \frac{C}{t} \tag{10}$$

which holds for all $a,t > 0$ and some constant C that depends only on the initial conditions $u(x,0) = \varphi(x)$. This condition restricts how large the positive secant slopes of u(x) can become in time, while the negative slopes remain unrestricted (Knobel 183).

α-Regularization Problem Statement and Conserved Quantities

Although many methods of approximation of solutions to conservation laws exist (Iserles, 1996; LeVeque, 1992), the purpose of this research is to test numerically several versions of what we call the α-regularizations of Burgers equation. Those regularizing schemes have been inspired by some of the recent sub-grid scale models of turbulence, such as the Navier-Stokes-α (and Euler-α) (Chen et al., 1999; Holm et al., 1998), the Leray-α (Cheskidov et al., 2005; Leray, 1934), and the modified Leray-α (Ilyin et al., 2006) models. The α-regularization has also been investigated in the context of the isentropic Euler equations (Bhat et al., 2007) For $0 \leq \theta \leq 1$ we consider:

$$v_t^\alpha + \theta\, u^\alpha v_x^\alpha + (1-\theta)\, u_x^\alpha v^\alpha = 0 \tag{11}$$

where v^α is related to u^α by:

$$v^\alpha = H[u^\alpha] \equiv u^\alpha - \alpha^2 u_{xx}^\alpha \tag{12}$$

with periodic boundary conditions $u^\alpha(x,t) = u^\alpha(x+L,t)$, $v^\alpha(x,t) = v^\alpha(x+L,t)$, and initial data:

$$v^\alpha(x,0) = v_0^\alpha(x) = \varphi(x) = \varphi(x+L) \tag{13}$$

The parameter θ can be chosen such that certain quantities are exactly conserved by (11). The conserved quantities for $\theta = 1, \frac{1}{3}, \frac{2}{3}$ are stated below in theorems 1, 2 and 3.

The Leray-α Model ($\theta = 1$)

For the case $\theta = 1$, one obtains the Leray-α regularization which was originally introduced by Jean Leray for the Navier Stokes equations governing incompressible fluid flow (Leray, 1934). This regularization scheme was proposed and studied by H. Bhat and R. Fetecau (Bhat and Fetecau, 2006) and E.Tadmor *et al.* (Tadmor et al., 2006). However in the numerical work of Bhat and Fetecau, the investigation did not conclusively demonstrate the convergence properties of the proposed scheme. In this paper, the convergence of functions $u^\alpha(x,t)$ and $v^\alpha(x,t)$ to the exact entropy solution $u(x,t)$ of the inviscid Burgers equation (2) is studied numerically as $\alpha \to 0$. If $\alpha = 0$ we formally have $v^\alpha = u^\alpha$ and the regularization problem becomes (2). For $\alpha \neq 0$, both functions $u^\alpha(x,t)$ and $v^\alpha(x,t)$ are smooth and do not have discontinuities, however in the limit as $\alpha \to 0$ there is recent evidence that solutions for $\theta = 1$ converge to possibly discontinuous entropy solutions of Burgers equation (Bhat and Fetecau, 2006; Tadmor et al., 2006).

If $\theta = 1$ the system (11)–(12) becomes:

$$v_t^\alpha(x,t) + u^\alpha(x,t)\,v_x^\alpha(x,t) = 0 \tag{14}$$

$$v^\alpha(x,t) = u^\alpha(x,t) - \alpha^2 u_{xx}^\alpha(x,t)$$

Define the L^p and L^∞ norms of a function $\psi \in L^p$ or $\psi \in L^\infty$ respectively:

$$\|\psi(x)\|_{L_p} \equiv \int_0^L |\psi(x)|^p\,dx, \text{ and } \|\psi(x)\|_{L_\infty} \equiv \sup_{x\in[0,L]}|\psi(x)| \tag{15}$$

Then for smooth enough initial data, it can be shown that the maximum and minimum of $v^\alpha(x,t)$ in (14) are conserved. In fact, one can show that:

$$\|v^\alpha(\cdot,t)\|_{L_\infty} = \|\varphi(\cdot)\|_{L_\infty} \tag{16}$$

Theorem 1 $\theta = 1$. *Let* $\varphi(x)$ *be smooth enough, and let* $u^\alpha(x,t)$, $v^\alpha(x,t)$ *be the corresponding L-periodic solutions of (14), then:*

$$\int_0^L v^\alpha(x,t)\,dx = \int_0^L \varphi(x)\,dx \tag{17}$$

That is, the total mass is conserved.

Proof. Integrate (14) by parts and apply the periodic boundary conditions to obtain:

$$\int_0^L v_t^\alpha(x,t) + u^\alpha(x,t)\,v_x^\alpha(x,t)\,dx = 0$$

$$\frac{d}{dt}\int_0^L v^\alpha(x,t)\,dx + \int_0^L u^\alpha(x,t)\,v_x^\alpha(x,t)\,dx = 0$$

$$\frac{d}{dt}\int_0^L v^\alpha(x,t)\,dx - \int_0^L u_x^\alpha(x,t)\,v^\alpha(x,t)\,dx = 0 \tag{18}$$

Applying (12), (18) leads to:

$$\frac{d}{dt}\int_0^L v^\alpha(x,t)\,dx - \int_0^L u_x^\alpha(x,t)\left\{u^\alpha(x,t) - \alpha^2 u_{xx}^\alpha(x,t)\right\}dx = 0$$

$$\frac{d}{dt}\int_0^L v^\alpha(x,t)\,dx - \int_0^L \frac{1}{2}\left\{(u^\alpha(x,t))^2\right\}_x - \frac{\alpha^2}{2}\left\{(u_x^\alpha(x,t))^2\right\}_x dx = 0$$

Applying periodic boundary conditions, the second integral vanishes and we have:

$$\frac{d}{dt}\int_0^L v^\alpha(x,t)\,dx = 0 \tag{19}$$

and integrating with respect to time, the result follows:

$$\int_0^L v^\alpha(x,t)\,dx = \int_0^L \varphi(x)\,dx$$

The α-Regularization Model With $\theta = \frac{1}{3}$

For $\theta = \frac{1}{3}$, the system (11)–(12) becomes:

$$v_t^\alpha(x,t) + \frac{1}{3}u^\alpha(x,t)\,v_x^\alpha(x,t) + \frac{2}{3}v^\alpha(x,t)\,u_x^\alpha(x,t) = 0 \tag{20}$$

$$v^\alpha(x,t) = u^\alpha(x,t) - \alpha^2 u_{xx}^\alpha(x,t)$$

Theorem 2 ($\theta = \frac{1}{3}$). *Let* $\varphi(x)$ *be smooth enough, and let* $u^\alpha(x,t)$, $v^\alpha(x,t)$ *be the corresponding L-periodic solutions of (20), then:*

$$\int_0^L (u^\alpha(x,t))^2 + \alpha^2 (u_x^\alpha(x,t))^2\,dx = \int_0^L (\varphi(x))^2 + \alpha^2(\varphi_x(x))^2\,dx \tag{21}$$

That is, a modified energy is conserved.

Proof. Multiply (20) by u^α and integrate:

$$0 = \int_0^L u^\alpha(x,t)\,v_t^\alpha(x,t)\,dx + \frac{1}{3}\int_0^L (u^\alpha(x,t))^2\,v_x^\alpha(x,t)\,dx +$$

$$+\frac{2}{3}\int_0^L v^\alpha(x,t)\,u^\alpha(x,t)\,u_x^\alpha(x,t)\,dx$$

$$= \int_0^L u^\alpha(x,t)\,v_t^\alpha(x,t)\,dx + \frac{1}{3}\int_0^L (u^\alpha(x,t))^2\,v_x^\alpha(x,t) +$$

$$+ v^\alpha(x,t)((u^\alpha(x,t))^2)_x\,dx$$

$$= \int_0^L u^\alpha(x,t)\,v_t^\alpha(x,t)\,dx + \frac{1}{3}\int_0^L ((u^\alpha(x,t))^2\,v^\alpha(x,t))_x dx$$

Applying boundary conditions, the last term is zero and we obtain:

$$\int_0^L u^\alpha(x,t)\,v_t^\alpha(x,t)\,dx = 0 \tag{22}$$

Plug (12) into (22) and we have:

$$\int_0^L u^\alpha(x,t)\, v_t^\alpha(x,t)\,dx = \int_0^L u^\alpha(x,t)\left\{u_t^\alpha(x,t) - \alpha^2 u_{xxt}^\alpha(x,t)\right\}dx$$

$$= \tfrac{1}{2}\tfrac{d}{dt}\int_0^L (u^\alpha(x,t))^2 + \alpha^2 (u_x^\alpha(x,t))^2\,dx = 0$$

that is:

$$\int_0^L (u^\alpha(x,t))^2 + \alpha^2 (u_x^\alpha(x,t))^2\,dx = \int_0^L (\varphi(x))^2 + \alpha^2 (\varphi_x(x))^2\,dx$$

The α-Regularization Model With $\theta = \frac{2}{3}$

For $\theta = \frac{2}{3}$, the system (11)–(12) becomes:

$$v_t^\alpha(x,t) + \tfrac{2}{3} u^\alpha(x,t) v_x^\alpha(x,t) + \tfrac{1}{3} v^\alpha(x,t) u_x^\alpha(x,t) = 0 \qquad (23)$$

$$v^\alpha(x,t) = u^\alpha(x,t) - \alpha^2 u_{xx}^\alpha(x,t)$$

Theorem 3 ($\theta = \frac{2}{3}$). *Let* $\varphi(x)$ *be smooth enough, and let* $u^\alpha(x,t)$, $v^\alpha(x,t)$ *be the corresponding L-periodic solutions of (23), then:*

$$\int_0^L \left|v^\alpha(x,t)\right|^2 dx = \int_0^L \left|\varphi(x)\right|^2 dx \qquad (24)$$

That is, the energy is conserved.

Proof. Multiply (23) by $v^\alpha(x,t)$ and integrate:

$$0 = \int_0^L v^\alpha(x,t)\, v_t^\alpha(x,t)\,dx + \tfrac{2}{3}\int_0^L v^\alpha(x,t) u^\alpha(x,t) v_x^\alpha(x,t)\,dx +$$

$$+ \tfrac{1}{3}\int_0^L (v^\alpha(x,t))^2 u_x^\alpha(x,t)\,dx$$

$$= \tfrac{1}{2}\int_0^L \left\{(v^\alpha(x,t))^2\right\}_t dx + \tfrac{1}{3}\int_0^L \left\{u^\alpha(x,t)(v^\alpha(x,t))^2\right\}_x dx$$

Applying boundary conditions, the last term is zero and we obtain:

$$\frac{1}{2}\frac{d}{dt}\int_0^L \left|v^\alpha(x,t)\right|^2 dx = 0 \qquad (25)$$

Finally applying initial condition (25) becomes:

$$\int_0^L \left|v^\alpha(x,t)\right|^2 dx = \int_0^L \left|\varphi(x)\right|^2 dx$$

Numerical Implementation

Consider the problem (11)–(13) with L-periodic initial conditions $v^\alpha(x,0) = v_o(x) = v_o(x+L)$. Create a fine mesh on the interval [0,1] such that $0 = x_0 < x_1 (= h) < x_2 (= 2h) < \ldots < x_N (= Nh) = L = 1$, where N and h are the number and size of the mesh in space respectively. Two initial profiles are considered to test the behavior of numerical solution:

$$v_0(x) = \varphi(x) = 1 - \cos(2\pi x) \qquad (26)$$

and

$$v_0(x) = \varphi(x) = \cos(2\pi x) \qquad (27)$$

In the former, the solution remains nonnegative and the shock moves; while in the latter, the solution has both positive and negative parts and the shock is stationary. The solution is computed up to a time t_f. Time is discretized as $0 = t_0 < t_1 (= \Delta t) < t_2 (= 2\Delta t) < \ldots < K\Delta t = t_f$, where K and Δt are the number and size of the time steps respectively. In particular $t_f = t_b$, $\frac{3}{2} t_b$ and $2t_b$ are considered, where t_b is the time at which the discontinuity of the solution of Burgers equation (2) forms and is given by equation (8). With this discretization define $u_j^n = u(x_j, t_n)$ and $v_j^n = v(x_j, t_n)$.

Equations (11) and (12) are solved simultaneously as a coupled system. Starting with initial conditions $v_o(x) = \varphi(x)$, evaluated at the mesh points, the values of $u_j^0 = u(x_j, 0)$, $j = 0, \ldots, N$ are obtained from (12) by means of the Finite Fourier Transform. Then at the first time step, $v_j^1 = v(x_j, \Delta t)$ is computed from equation (11) using the Forward Time Centered Space (FTCS) spatial discretization scheme. However this method is actually unstable for use at long times and so the further time steps are computed using second order multistep Leap Frog scheme (Strikwerda, 2004). The solution is computed by going back and forth between equations (11) and (12) at each time step.

Solution to $u(x,t) - \alpha^2 u_{xx}(x,t) = v(x,t)$ *at each time step.* Several methods could be used to compute $u(x,t_n)$ given $v(x,t_n)$ for each fixed t_n from (12) such as the Thomas algorithm (Strikwerda 88) applied to finite difference methods (Thomas, 1995), and the spectral method based on the Finite/Fast Fourier Transform (Strikwerda 46). Here we use a spectral method where the Complex Split Radix Fast Fourier Transform (FFT) subroutine (Kifowit, 2005) was used to implement the Finite Fourier Transform. This approach gives a smaller maximum L_1 error compared to the Finite Difference algorithm using the Thomas solution method. The forward Finite Fourier Transform is defined as:

$$\hat{u}_k = \sum_{j=0}^{N-1} u_j e^{-2\,ijk\pi h} \qquad (28)$$

and the backward Finite Fourier Transform is given by:

$$u_j = h\sum_{k=0}^{N-1} \hat{u}_k e^{2\,ijk\pi h} \qquad (29)$$

Given $v(x,t_n)$ at the mesh points for a fixed time, the forward transform gives an array $\hat{v}_k, k=0,\ldots,N-1$. Using the derivative formula for the Finite Fourier transform and shifting indices, equation (12) becomes:

$$\sum_{k=0}^{N-1}\hat{v}_k e^{2ij(k-N/2)\pi h}=\sum_{k=0}^{N-1}\hat{u}_k e^{2ij(k-N/2)\pi h}+\sum_{k=0}^{N-1}4(\alpha(k-N/2)\pi)^2\,\hat{u}_k e^{2ij(k-N/2)\pi h}$$

Matching coefficients, this gives $\hat{u}_k$ in terms of known quantities (Thomas 101):

$$\hat{u}_k=\frac{\hat{v}_k}{1+4\alpha^2\pi^2(k-N/2)^2},\quad k=0,\ldots,N-1 \tag{30}$$

Then using backward transform (29), $u(x,t_n)$ is obtained for that time step t_n.

Difficulties with this method might arise due to the occurrence of aliasing instabilities over long times for large N (Boyd, 2001). In this case some smoothing of the high modes of the Fourier spectrum is required. Aliasing instability here is controlled by using 25th order Fourier filtering to damp the highest modes (Hou et al., 1994):

$$\Pi[\hat{v}_k]=e^{-10(|k|/N)^{25}}\hat{v}_k \tag{31}$$

The overall accuracy of the method is determined by the filter and is of order $O((1/N)^{25})$ (Hou et al.,1994). To reduce the noise introduced by taking derivatives, Krasny filtering was also used, where the Fourier modes of magnitude less than the tolerance level $\varepsilon=10E-12$ were set to zero (Krasny, 1986). The combination of both methods, when applied to $\hat{v}_k$ before evaluating $\hat{u}_k$ from (30), significantly improves the accuracy of the method.

First Time Step FTCS (Forward Time Centered Space) Scheme. In this scheme forward and center difference formulas are used to discretize time and space derivatives respectively (Strikwerda 17):

$$\frac{d}{dt}v_j^n=\frac{v_j^{n+1}-v_j^n}{\Delta t}+O(\Delta t)\approx\frac{v_j^{n+1}-v_j^n}{\Delta t} \tag{32}$$

$$\frac{d}{dx}u_j^n=\frac{u_{j+1}^n-u_{j-1}^n}{2h}+O(h^2)\approx\frac{u_{j+1}^n-u_{j-1}^n}{2h} \tag{33}$$

Using (32) and (33), equation (11) becomes:

$$\frac{v_j^1-v_j^0}{\Delta t}+\theta u_j^0\left(\frac{v_{j+1}^0-v_{j-1}^0}{2h}\right)+(1-\theta)v_j^0\left(\frac{u_{j+1}^0-u_{j-1}^0}{2h}\right)=O(\Delta t)+O(h^2)$$

which solving for v_j^1, and dropping the error terms, gives:

$$v_j^1=v_j^0-\frac{\Delta t}{2h}(\theta u_j^0(v_{j+1}^0-v_{j-1}^0)+(1-\theta)v_j^0(u_{j+1}^0-u_{j-1}^0)) \tag{34}$$

Knowing v_j^0 and u_j^0, equation (34) gives v_j^1 for the next time iteration $\forall j=0,1,\ldots,N$. This scheme is used on the first time step only to provide enough information for employing the multistep Leap Frog scheme for the remaining time steps.

Time Steps for n > 1 Leap Frog CTCS (Centered Time Centered Space) Scheme. In this scheme center difference formulas are used to discretize both time and space derivatives (Strikwerda 17), i.e.:

$$\frac{d}{dt}v_j^n=\frac{v_j^{n+1}-v_j^{n-1}}{2\Delta t}+O(\Delta t^2)\approx\frac{v_j^{n+1}-v_j^{n-1}}{2\Delta t} \tag{35}$$

Using (35) and (33), equation (11) becomes:

$$\frac{v_j^{n+1}-v_j^{n-1}}{2\Delta t}+\theta u_j^n\left(\frac{v_{j+1}^n-v_{j-1}^n}{2h}\right)+(1-\theta)v_j^n\left(\frac{u_{j+1}^n-u_{j-1}^n}{2h}\right)=O(\Delta t^2)+O(h^2)$$

which solving for v_j^{n+1}, and dropping the error terms as before, gives:

$$v_j^{n+1}=v_j^{n-1}-\frac{\Delta t}{h}(\theta u_j^n(v_{j+1}^n-v_{j-1}^n)+(1-\theta)v_j^n(u_{j+1}^n-u_{j-1}^n)) \tag{36}$$

Therefore, knowing v_j^n, u_j^n and v_j^{n-1}, equation (36) gives v_j^{n+1} for the next time iteration $\forall j=0,1,\ldots,N$.

Stability and Convergence. For an explicit numerical scheme one of the necessary stability conditions is Courant-Friedrichs-Lewy condition (Strikwerda 34) stating that the ratio $\frac{\max|u^n|\Delta t}{h}<1$. Physically this means that the solution (e.g. shock wave) can not propagate more than one grid spacing in a single time step. Here, since $\max|u^n|\approx 1$ by choice of initial conditions, the following stability relation was used:

$$\Delta t=\frac{h}{2} \tag{37}$$

Since the parameter α is a key convergence parameter, we use the following criteria to determine physically reasonable choices of α. For example, when $\theta = 1$, the maximum of $v^\alpha(x,t)$ is conserved in time and thus cannot exceed the maximum in the initial data. However, for a fixed number of partition intervals N considered, there is a particular value of α below which $v^\alpha(x)$ becomes oscillatory, hence violating maximum conservation condition. One of the tasks of this numerical investigation was to establish a relation between α and the mesh size that preserves stability and consistency with Theorems 1–3. For the case $\theta = 1$,

holding N fixed, α is decreased incrementally while the maximum of the numerical approximation of $v^{\alpha}(x,t)$ lies within a specified tolerance level δ of the maximum of the initial data. That is, α can only be decreased as long as the following condition holds:

$$\left|\max_{j=1,\ldots,N}\left|v(x_j,t_n)\right| - \max_{j=1,\ldots,N}\left|\varphi(x_j)\right|\right| \le \delta \qquad (38)$$

for all discrete times $t_n \le t_f$.

For the remaining cases $\theta = \frac{1}{3}$ and $\theta = \frac{2}{3}$ the maximum of $v^{\alpha}(x,t)$ need not be conserved and the stopping criteria for decreasing α relies on the results of Theorems 2 and 3. The conserved quantities (21) and (24) are computed numerically for $\theta = \frac{1}{3}$ and $\theta = \frac{2}{3}$ respectively. Using the derivative approximation (33) they become:

$$h\left(\sum_{j=1}^{N}(u_j^n)^2 + \alpha^2\left(\frac{u_{j+1}^n - u_{j-1}^n}{2h}\right)^2\right) = \text{const} \qquad (39)$$

and

$$h\left(\sum_{j=1}^{N}\left|v_j^n\right|^2\right) = \text{const} \qquad (40)$$

Holding N fixed, α is decreased incrementally while the numerical approximation of the conserved quantity (39) or (40) (depending on θ) lies within a specified tolerance level δ of the initial value for all $t_n \le t_f$. That is, α can only be decreased as long as the numerical equivalents of Theorems 2 and 3 are satisfied.

Exact Solution

The numerically computed solution is compared to the exact entropy solution obtained by the method of characteristics for the two different initial data (26) and (27).

The discontinuity is calculated from (8) to occur at $t_b = \frac{1}{2\pi}$ for both cases. For $t < t_b$ and $x \in [0,1]$ the continuous solution is found in the same way for both (26) and (27) using equations (4) and (5) and applying Newton's iteration method. The initial guess is randomly chosen in the interval [0,1] and the iteration is repeated until x_o converges to an element of [0,1]. However after the break time a different approach must be used because the characteristics intersect (shock formation).

In the case of the initial data given in equation (26) the shock forms at $(x_b,t_b) = (\frac{2+3\pi}{4\pi}, \frac{1}{2\pi})$ and the characteristic that initiates the shock originates from $x_o^b = \frac{3}{4}$. Suppose at the break time the speed of the shock, given by (7), is $\dot{x}_s(t_b) \approx \frac{1}{2}(\varphi(x_o^b) + \varphi(x_o^b)) = 1$. At the later times the position of the shock is computed as:

$$x_s(t_b + \Delta tk) = x_b + (\Delta x)_1 + \ldots + (\Delta x)_k \qquad (41)$$

where

$$(\Delta x)_k \approx \dot{x}_s(t_b + \Delta t(k-1))\Delta t \qquad (42)$$

where the error is $O(\Delta t^2)$, and from Rankine-Hugoniot condition (7):

$$\dot{x}_s(t_b + \Delta t(k-1)) = \frac{1}{2}(u^+(t_b + \Delta t(k-1)) + u^-(t_b + \Delta t(k-1))) \qquad (43)$$

Knowing the position of the shock at each time step allows for the successful choice of the initial guess in the Newton iteration algorithm when solving equation (4) for x_o. Characteristics starting to the right of x_o^b carry the values of $u(x, t_b + \Delta tk)$ only for x to the right of $x_s(t_b + \Delta tk)$ and the characteristics to the left of x_o^b carry the values of $u(x, t_b + \Delta tk)$ for x to the left of $x_s(t_b + \Delta tk)$.

In the case of the initial data in equation (27) the shock is stationary and is located at $x = \frac{1}{4}$; hence we do not need to use (7) to determine the change in the shock position in time. However, more intervals need to be considered (i.e., [-1/4, 1/4], [1/4, 3/4], [3/4, 5/4]) for the initial guess generation for the Newton iteration of equation (4) given $(x,t) \in [0,1] \times [0,t_f]$.

Once the exact entropy solution is obtained, the L_1 error is calculated at each fixed time as:

$$E(t_n)[u^{\alpha}] = h\sum_{j=1}^{N}\left|u^{\alpha}(x_j,t_n) - u_j^n\right| \qquad (44)$$

where $u_{i,j}$ is the exact entropy solution computed as described above. The global error is computed as a maximum L_1 error over all times up to t_f:

$$E[t_f] = \max_{n=1,\ldots,K}\left|E(t_n)\right| \qquad (45)$$

Results and Discussion

The Case of $\theta = 1$

For the initial data (26) the solution is nonnegative and the nonzero parts of the solution move to the right in time at different speeds; however, for the initial data (27) the position of the shock is fixed at $x = \frac{1}{4}$. Figures 1 and 2 show the exact and numerical solution curves superimposed for

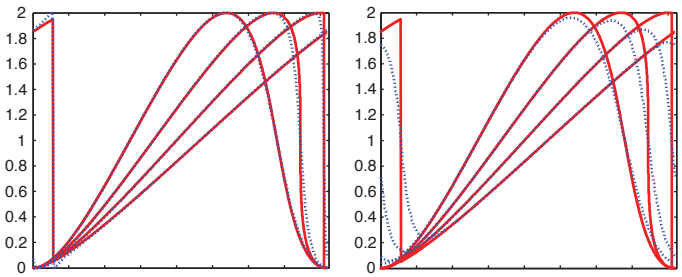

Figure 1

Solution curves computed up to $t = 2t_b$ for the initial data (26). Red solid curves represent the exact solution for $t = (1/2)t_b, t_b, (3/2)t_b$ and $2t_b$. Blue dotted curves represent the corresponding numerical solution: [A]-$v^\alpha(x)$, [B]-$u^\alpha(x)$ with N=16384 and α=0.0327.

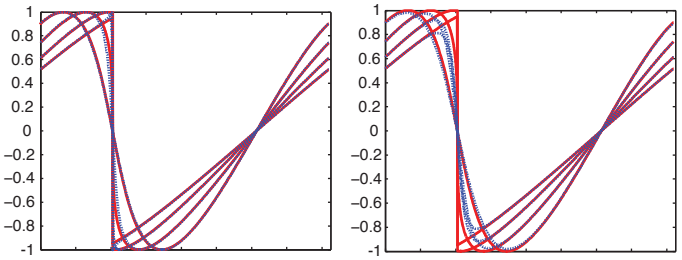

Figure 2

Solution curves computed up to $t = 2t_b$ for the initial data (27). Red solid curves represent the exact solution for $t = (1/2)t_b, t_b, (3/2)t_b$ and $2t_b$. Blue dotted curves represent the corresponding numerical solution: [A]-t, [B]-$u^\alpha(x)$ with N=16384 and α=0.0216.

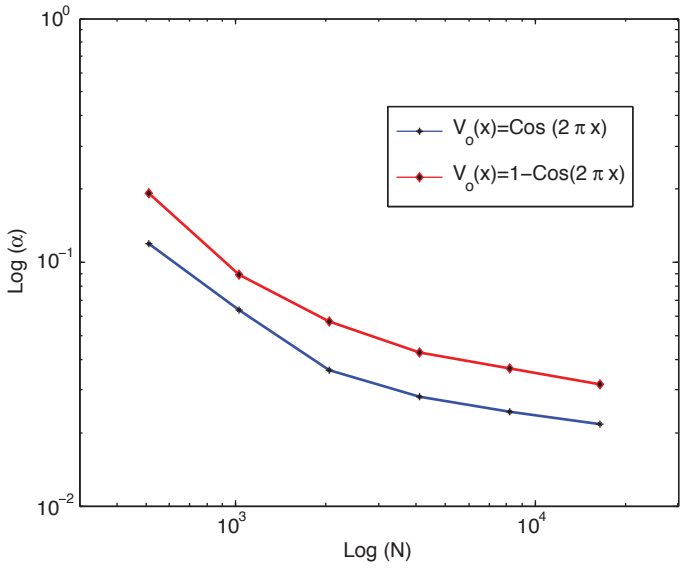

Figure 3

Relationship between α and N for θ = 1 computed up to $t = 2t_b$ (twice the break time).

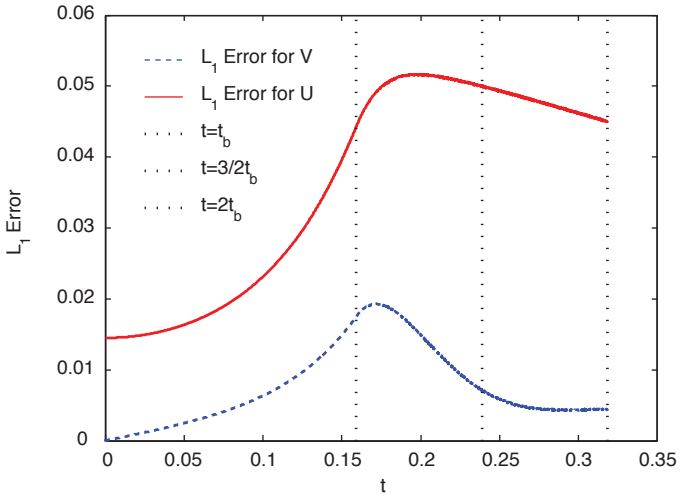

Figure 4

Local L_1 Error (44) as a function of time computed for both u^α and v^α up to $t_f = 2t_b$ with N=8192 and α=0.0243, $V_o(x) = \mathrm{Cos}(2\pi x)$.

$v^\alpha(x,t)$ and $u^\alpha(x,t)$ for both initial conditions. Observe that up to time $t = 3/2t_b$, v^α is an excellent approximation of the exact solution. The function u^α also approximates the exact solution but is smoothed over a larger region and deviates more near the discontinuity. At larger times, for example $t = 2t_b$, it is apparent that v^α does not decay while both the exact solution and u^α do decay. This will be important later when we check the Oleinik entropy inequality.

The tolerance level $\delta = 10E-5$ is used with equation (38) to generate a relationship between α and $N = \frac{1}{h}$ computed up to twice the break time. This relationship is shown on Figure 3 in log-log scale for both initial conditions (26) and (27). The physically meaningful α lie above the curves. For combinations of α and $\frac{1}{h}$ below the curves, oscillations will develop in the numerical solution and the maximum of v^α will no longer be conserved.

The local L_1 error (44) as well as the global L_1 error (45) were computed. Figure 4 shows the evolution of L_1 error in time for N=8192 for the case of the initial data in (27). The vertical lines mark the times t_b, $\frac{3}{2}t_b$ and $2t_b$. Observe that the maximum error occurs just after the break time. Note that the error for v^α is significantly less than the error for u^α. However, around time $t = 2t_b$, the error in v^α begins to increase in time due to the fact that v^α does not decay, which violates the entropy condition (10).

In Figures 5A and 5B the global error up to $t = \frac{3}{2}t_b$ and $t = 2t_b$, as well as the local error at $t = t_b$, is shown as a function of α for both initial conditions (26) and (27). In all cases the rate of convergence in α is approximately 1 or better for

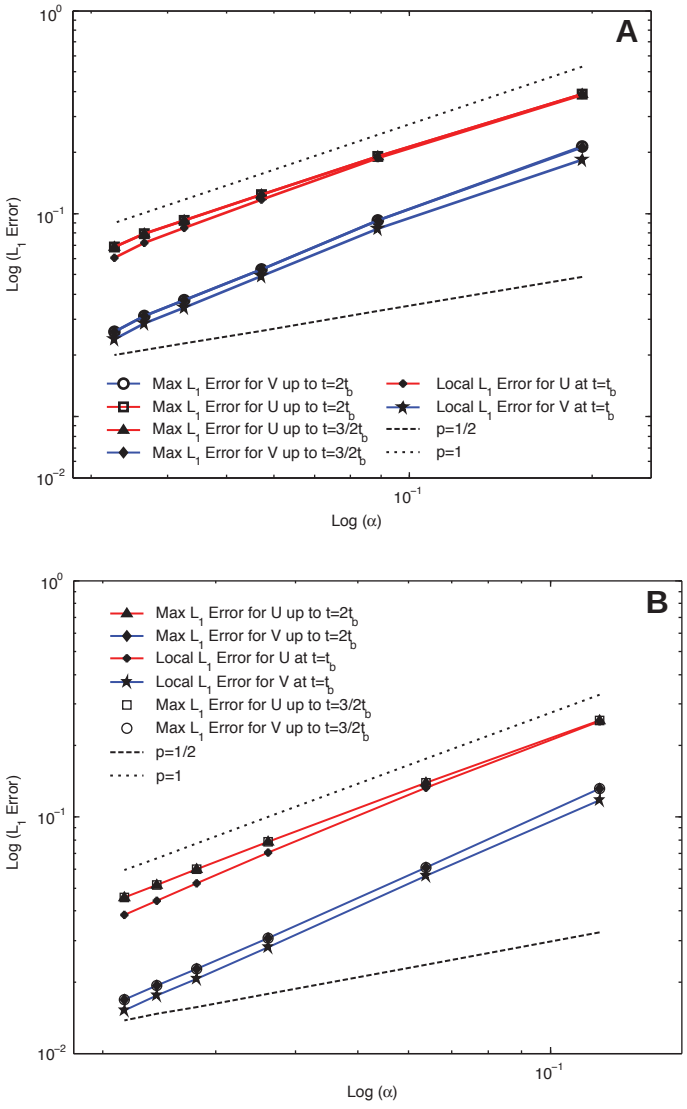

Figure 5

[A]: Relationship between global (max) and local L_1 error and α for θ = 1 and initial condition (26). [B]: Relationship between global (max) or local L_1 error and α for θ = 1 and initial condition (27). (The reference slope lines are indicated by p = 1 and p = 1/2.)

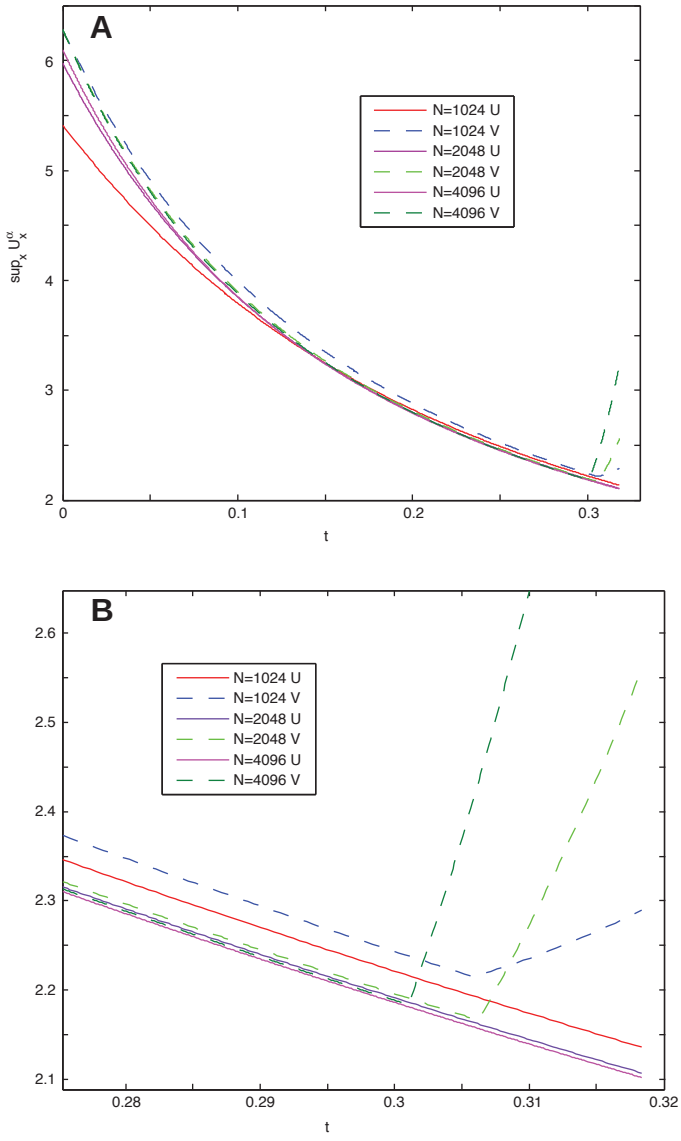

Figure 6

[A]: Oleinik Inequality (46) plotted for θ = 1 and initial condition $v_o = \mathrm{Cos}(2\pi x)$, [B]: Zoom in on the area where v^α starts violating the entropy condition.

the error in u^α and v^α. The reference lines indicating convergence rates (i.e. $E \sim \alpha$) for p = 1 (dashed) and p = 1/2 (dash-dot) are also shown in Figures 5A and 5B.

Equation (10) is used to check if the numerical solution satisfies the entropy condition. The equivalent representation of Oleinik inequality that is easier to check numerically is:

$$\max_{x_i} \frac{v^\alpha(x_{i+1},t) - v^\alpha(x_i,t)}{h} < \frac{C}{t}, \quad i = 0,\ldots,N-1 \qquad (46)$$

Figures 6 and 7 show that the positive slopes are bounded for both types of initial conditions (26) and (27) for $u^\alpha(x,t)$. Therefore it appears that the numerical solution $u^\alpha(x,t)$ does satisfy the entropy condition, thus suggesting convergence to the unique physical solution. Interestingly, from Figures 6 and 7 it appears that v^α does not satisfy the Oleinik inequality. Note that as the mesh is refined, the rapid growth in v^α_x occurs earlier in time suggesting that v^α violates Oleinik inequality in the limit $h \to 0$. The general question of convergence of discrete solutions to the continuous entropy solution strongly depends on the choice of numerical scheme. We conjecture that the only appropriate numerical schemes for which v^α converges to the entropy solution are of upwind-type, which will yield convergence to the entropy solution as $h \to 0$ even if $\alpha = 0$.

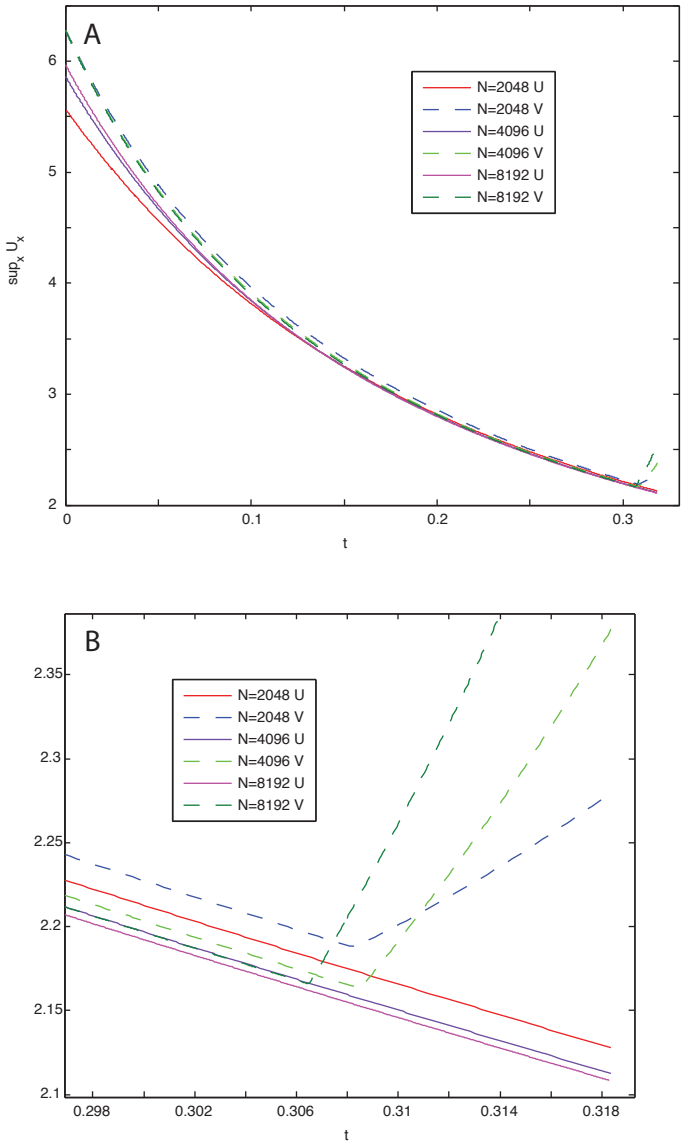

Figure 7

[A]: Oleinik Inequality (46) plotted for $\theta = 1$ and initial condition $v_o = 1 - \mathrm{Cos}(2\pi x)$, [B]: Zoom in on the area where v^α starts violating the entropy condition.

As an additional check of accuracy, (17) was computed numerically at each time step. The difference between (17) at time zero and (17) at any other time step did not exceed 1E−8, hence implying that the numerical scheme also conserves this quantity.

The Case of $\theta = \frac{2}{3}$

We next consider the case in which $\theta = \frac{2}{3}$. Here, the stopping criterion:

$$\left| h\sum_{i=0}^{N-1}(v^\alpha(x_i,t_j))^2 - h\sum_{i=0}^{N-1}(v^\alpha(x_i,0))^2 \right| \le \delta \qquad (47)$$

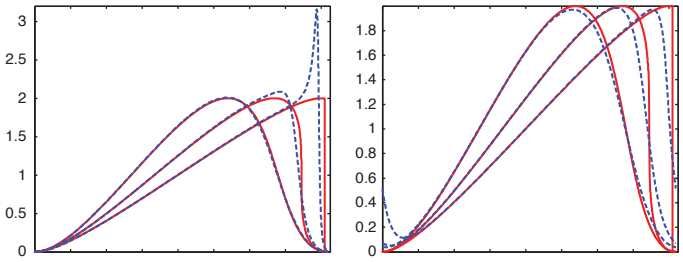

Figure 8

($\theta = \frac{2}{3}$): Solution curves computed up to $t = \frac{3}{2}t_b$ for the initial data (26). Red solid curves represent the exact solution for $t = (1/2)t_b, t_b, (3/2)t_b$. Blue dotted curves represent the corresponding numerical solution: [A]-$v^\alpha(x)$, [B]-$u^\alpha(x)$ with $N = 16384$ and $\alpha = 0.0297$.

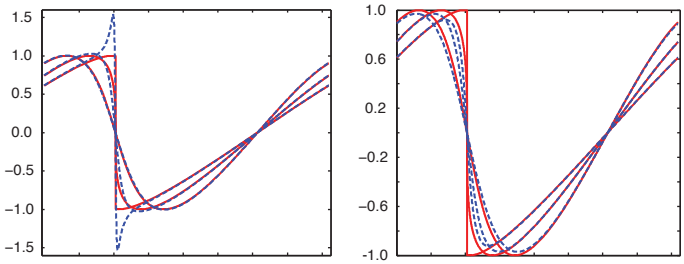

Figure 9

($\theta = \frac{2}{3}$): Solution curves computed up to $t = \frac{3}{2}t_b$ for the initial data (27). Red solid curves represent the exact solution for $t = (1/2)t_b, t_b, (3/2)t_b$. Blue dotted curves represent the corresponding numerical solution:[A]-$v^\alpha(x)$, [B]-$u^\alpha(x)$ with $N = 16384$ and $\alpha = 0.0281$.

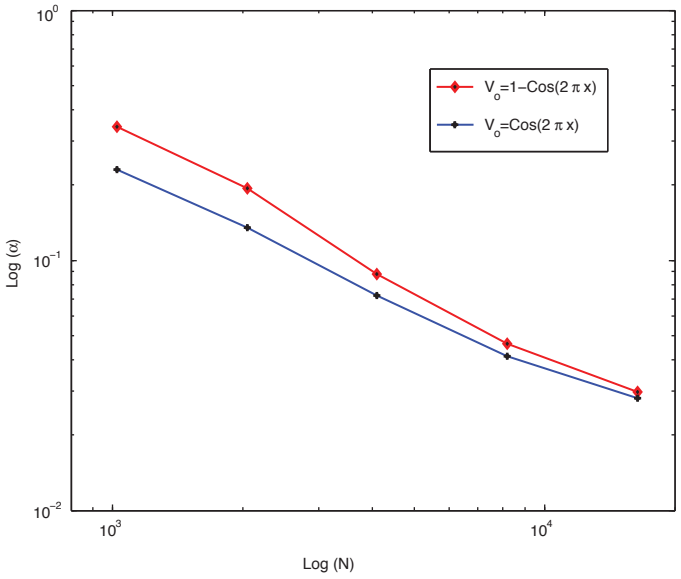

Figure 10

Relationship between α and N for $\theta = \frac{2}{3}$ computed up to $\frac{3}{2}$ break time.

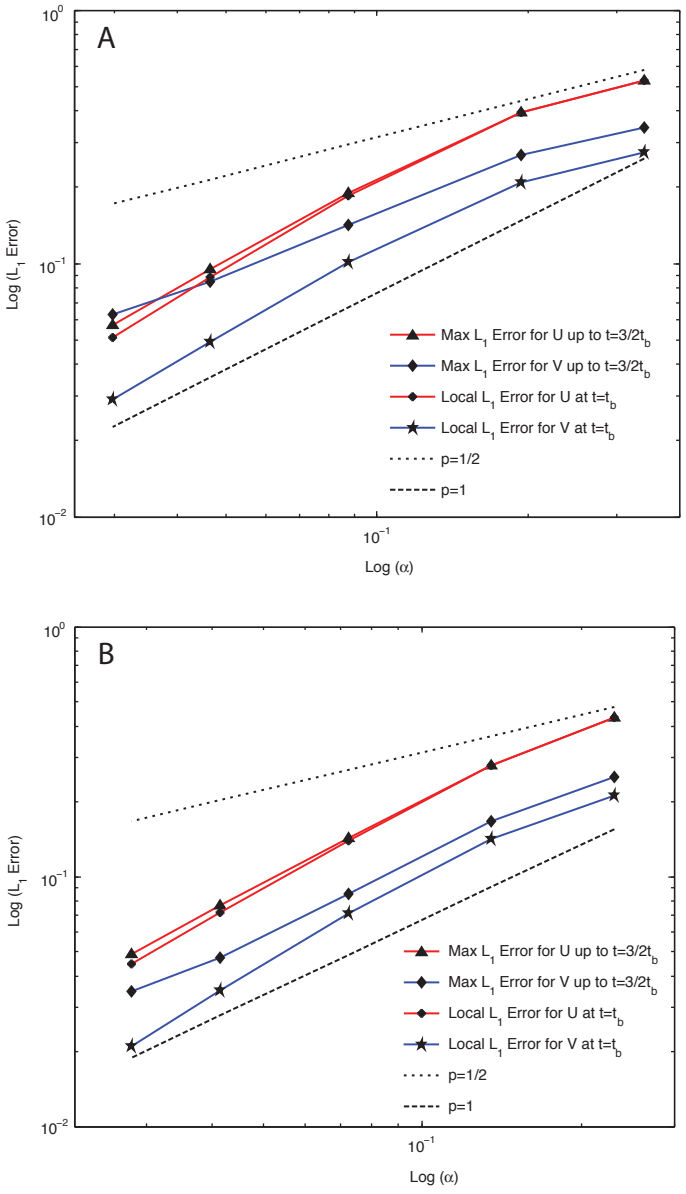

Figure 11

[A]: Relationship between global (max) or local L_1 error and α for $\theta=\frac{2}{3}$ and initial condition $v_o(x)=1-\mathrm{Cos}(2\pi x)$. [B]: Relationship between global (max) or local L_1 error and α for $\theta=\frac{2}{3}$ and initial condition $v_o=\mathrm{Cos}(2\pi x)$. (The reference slope lines are indicated by p = 1 and p = 1/2.)

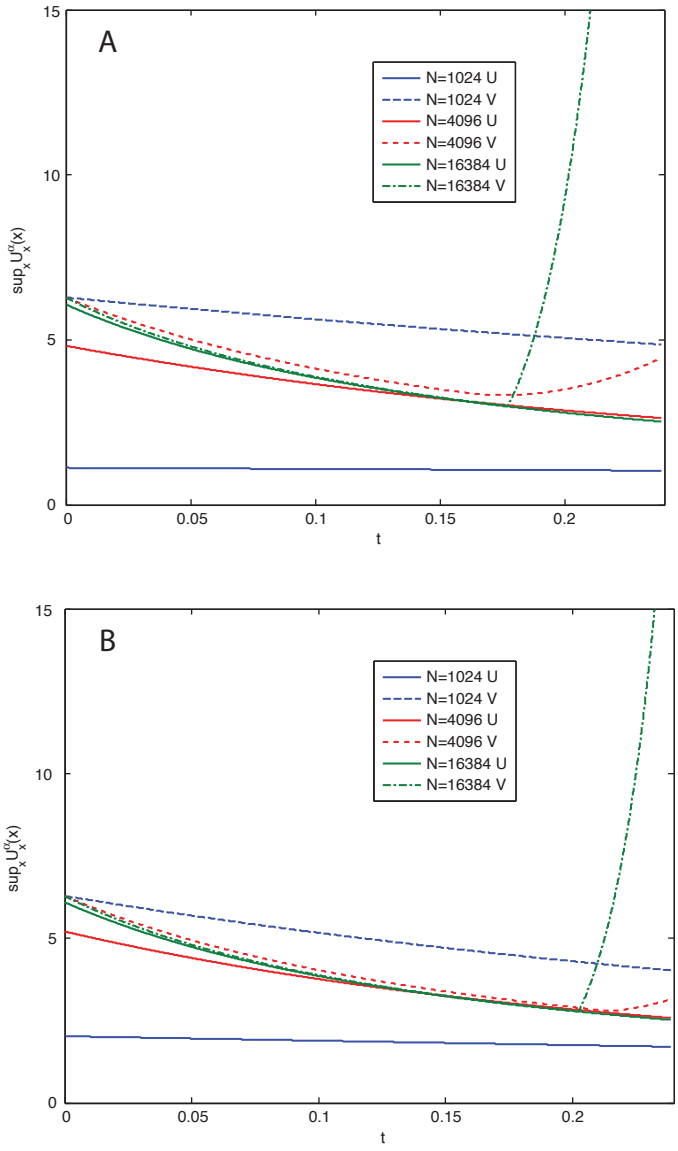

Figure 12

Oleinik Inequality (46) plotted for $\theta=\frac{2}{3}$ and initial conditions (26)-[A] and (27)-[B].

is used to determine the range of physically relevant α. Figures 8 and 9 show the numerical solution curves for u^α and v^α computed using $\theta=\frac{2}{3}$ and α as labeled. Observe that v^α has large overshoots near the discontinuity and the function u^α provides a better approximation of the exact physically meaningful solution.

The numerical investigation shows that for a given N, the parameter α cannot be decreased indefinitely without violating Theorem 3. The relationship between α and N is established as described previously using (47) with the tolerance level $\delta=10E-7$. The plot of this relationship is presented in Figure 10. Analogously to the case of $\theta=1$, the physically meaningful α lie above the curves. For the combinations of α and N below the curves, the energy (40) is not conserved in time to the tolerance level specified above, thus violating Theorem 3 and therefore not providing a valid solution to the modeled problem.

Figures 11A and 11B show the relationships between the global error up to $t=\frac{3}{2}t_b$ as well as the local error at t_b as a function of α for both initial conditions (26) and (27) respectively. Both initial conditions demonstrate the same convergence behavior in α. For small α (large N) the order

of convergence in α is about 1.2 for local error at $t = t_b$ for both v^α and u^α. The same is true for global error for u^α. However, the global error for v^α does not seem to settle to a linear profile in log-log scale for small α and instead the order of convergence decreases, implying that v^α does not converge to the exact solution as fast as u^α or perhaps does not converge at all.

To check if the numerically computed solutions satisfy the entropy condition, the Oleinik inequality is plotted in Figure 12 for both initial conditions. As in the $\theta = 1$ case, the positive slopes of u^α for $\theta = \frac{2}{3}$ seem to be bounded for both initial conditions, thus implying that the solution appears to satisfy the entropy condition and is physically meaningful. However for v^α the positive slopes become unbounded for larger t causing v^α to violate the entropy condition. Further, as in the $\theta = 1$ case, the rapid growth of v_x^α occurs at earlier times when the mesh is refined.

Both error and entropy investigation imply that it is u^α that appears to converge to the unique entropy solution and not v^α. As is clearly visible from the plots of the numerical solution for both initial data the oscillations and sharp positive gradients appear around the shock in the case of v^α. This causes the error to grow and results in the violation of the entropy condition for v^α. The function u^α on the other hand is monotone around the region of discontinuity in exact solution and appears to converge steadily without violating the entropy condition.

The Case of $\theta = \frac{1}{3}$

Figures 13 and 14 show the numerical approximations u^α and v^α computed using $\theta = \frac{1}{3}$. It is clear that the solution is well approximated only for regions that are far away from the position of the discontinuity in the exact solution. Oscillations and overshoots develop in both v^α and u^α in this case, and the growth of positive slopes is visible even from the solution curves for as early as $t = t_b$.

The tolerance level $\delta = 10E-7$ is used with equation (39) to generate a relationship between α and $N = \frac{1}{h}$ computed up to $t = \frac{3}{2}t_b$. This relationship is shown in Figure 15 in log-log scale for both initial conditions (26) and (27). As in the previous cases, the physically meaningful α lie above the curves. For the combinations of α and N below the curves, the modified energy (39) is not conserved in time to the tolerance level specified above, thus violating Theorem 2 and therefore not providing an accurate solution to the modeled problem.

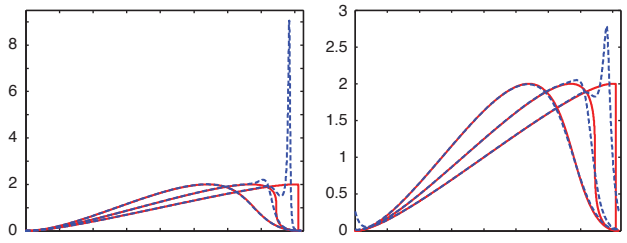

Figure 13

($\theta = \frac{1}{3}$) Solution curves computed up to $t = \frac{3}{2}t_b$ for the initial data (26). Red solid curves represent the exact solution for $t = (1/2)t_b, t_b, (3/2)t_b$. Blue dotted curves represent the corresponding numerical solution: [A]-$v^\alpha(x)$, [B]-$u^\alpha(x)$ with N=16384 and α=0.0175.

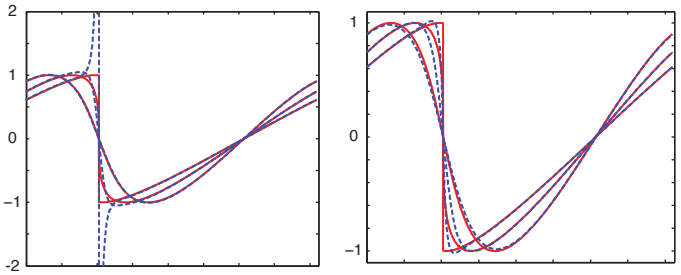

Figure 14

($\theta = \frac{1}{3}$) Solution curves computed up to $t = \frac{3}{2}t_b$ for the initial data (27). Red solid curves represent the exact solution for $t = (1/2)t_b, t_b, (3/2)t_b$. Blue dotted curves represent the corresponding numerical solution: [A]-$v^\alpha(x)$, [B]-$u^\alpha(x)$ with N=16384 and α=0.0226.

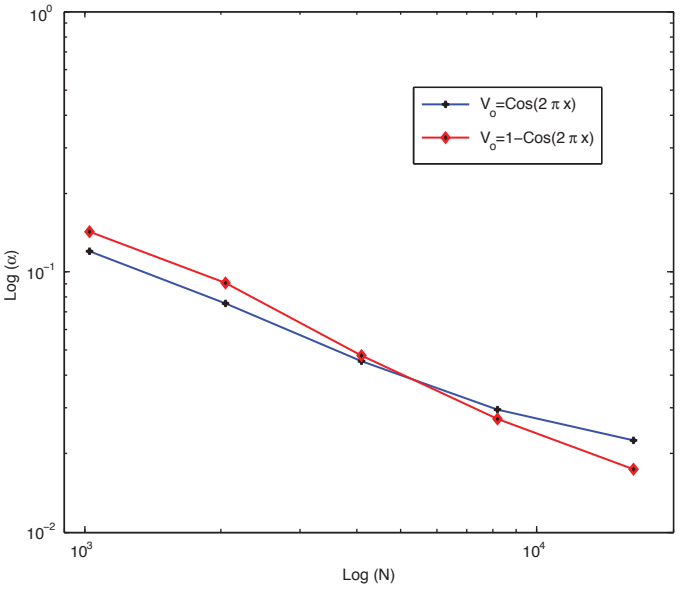

Figure 15

Relationship between α and N for ($\theta = \frac{1}{3}$) computed up to $\frac{3}{2}$ break time.

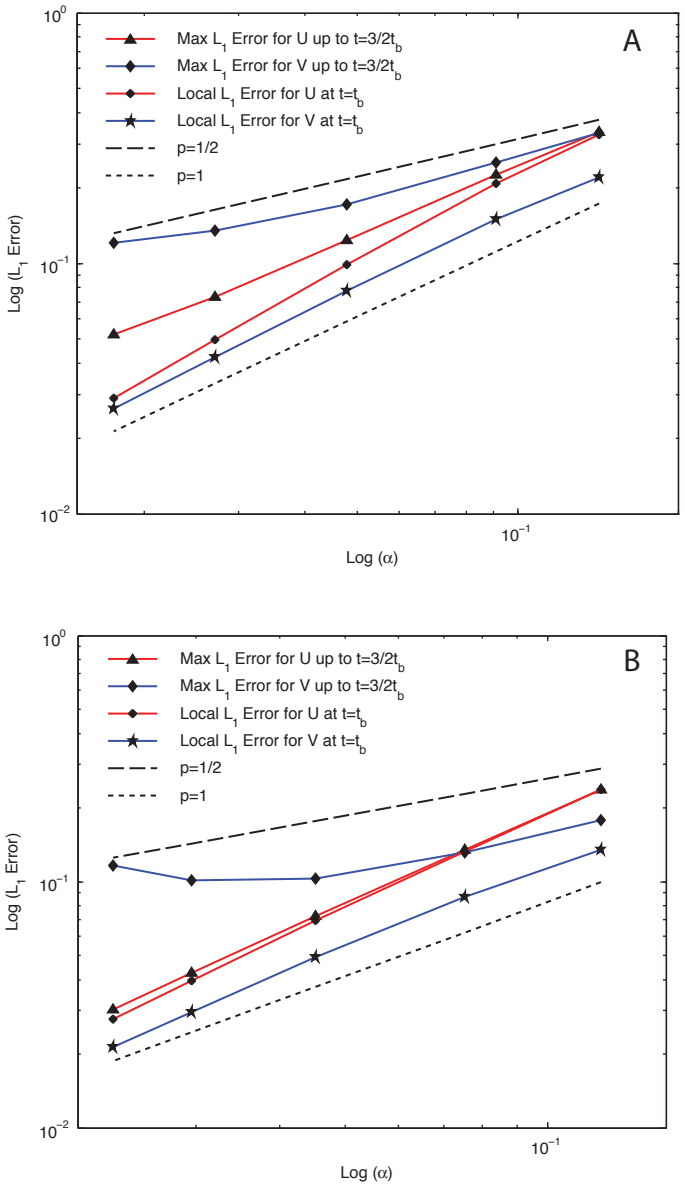

Figure 16

[A]: Relationship between global (max) or local L_1 error and α for ($\theta = \frac{1}{3}$) and initial condition $v_0(x) = 1 - \mathrm{Cos}(2\pi x)$. [B]: Relationship between global (max) or local L_1 error and α for ($\theta = \frac{1}{3}$) and initial condition $v_0 = \mathrm{Cos}(2\pi x)$. (The reference slope lines are indicated by p = 1 and p = 1/2.)

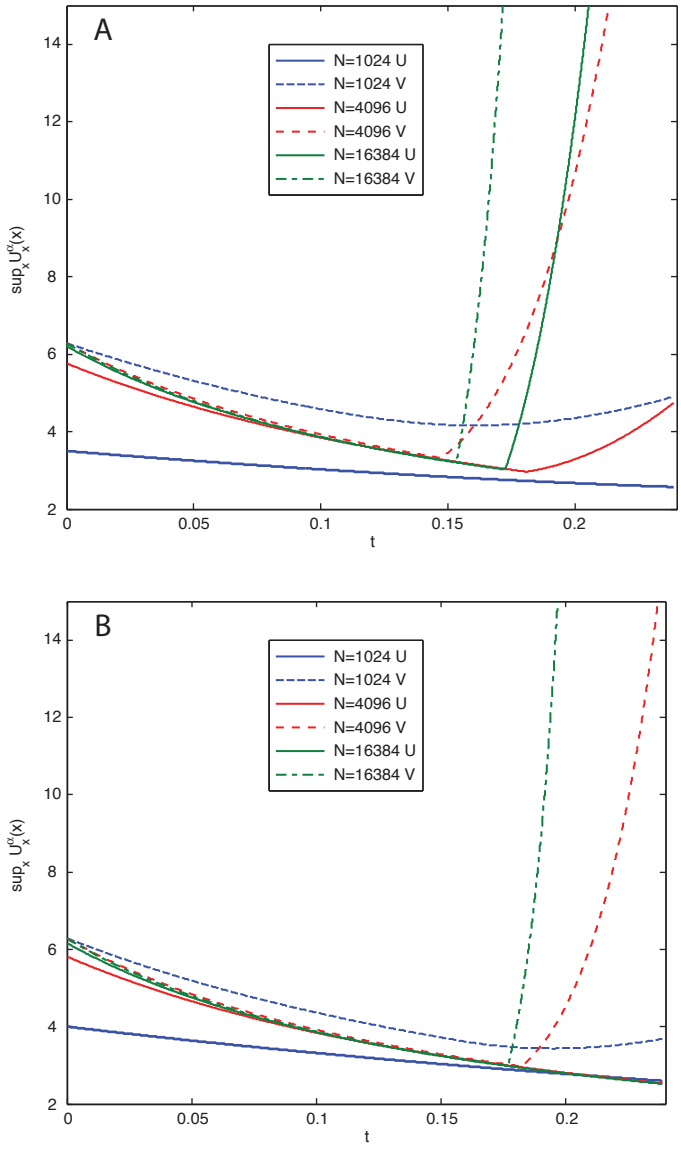

Figure 17

Oleinik Inequality (46) plotted for ($\theta = \frac{1}{3}$) and initial conditions (26)-[A] and (27)-[B].

Figures 16A and 16B show the relationships between the global and local errors up to $t = \frac{3}{2}t_b$ as a function of α for both initial conditions (26) and (27) respectively. The order of convergence in α for large N of the local L_1 error at break time is about 1.2 for u^α and 1 for v^α for initial conditions (26). For the other initial condition (27) the order is about 1.3 for u^α and 1.2 for v^α. However, the global error, does not appear to settle to a linear log-log profile consistently for both initial data for both u^α and v^α. Thus at the later times after the shock forms in the exact solution, neither v^α nor u^α converges at a constant rate to the exact solution. In fact, the convergence rate in α decreases and the solution apparently diverges.

To check if the numerically computed solutions satisfy the entropy condition, the Oleinik inequality is plotted in Figure 17 for both initial data. Unlike the previous cases of $\theta = 1$ and $\theta = \frac{2}{3}$, the positive slopes of u^α for $\theta = \frac{1}{3}$ also become unbounded, for at least one of the initial conditions (26). This implies that neither u^α nor v^α satisfy the entropy condition and both numerical solutions are not physically meaningful in the limit $h \to 0$.

Conclusion

We have solved Burgers equation using the Leray-α regularization numerically using a hybrid algorithm combining a finite difference scheme for the conservation law and the spectral method for the regularization. We examined the results for two types of periodic initial data. For both types of initial data considered, shocks form. In one case the shock moves, while the shock is stationary in the other. For both initial data and for $\theta = 1$ and $\frac{2}{3}$, we find numerical convergence of the regularized solution u^α to the unique entropy solution of the Burgers equation. However, v^α was apparently in violation of the entropy condition in all the cases considered. Hence, v^α seemingly does not represent a physically meaningful solution to Burgers equation in the limit $h \to 0$. For $\theta = \frac{1}{3}$ it appears that for the given numerical scheme used, neither u^α nor v^α converge to the unique entropy solution. Further study of this regularization scheme could be done employing different numerical approaches to determine whether there are schemes for which v^α converges to the entropy solution. We suggest that such schemes are of upwind type and would thus give convergence to the entropy solution even if $\alpha = 0$. Centered difference schemes of the type used here likely do not enable v^α to converge to the entropy solution.

Acknowledgements

The author thanks her advisors Professor John Lowengrub and Professor Edriss S. Titi from the UCI Mathematics Department. The author also gratefully acknowledges support from the University of California, Irvine Undergraduate Research Opportunities Program and the National Science Foundation.

Works Cited

Bhat, Harish and Razvan Fetecau. "A Hamiltonian Regularization of the Burgers Equation." Journal of Nonlinear Science. 16.6 (2006): 615–638.

Bhat, Harish, Razvan Fetecau and Jonathan Goodman. "A Leray-Type Regularization for the Isentropic Euler Equations." Nonlinearity. 20 (2007): 2035–2046.

Boyd, John. Chebyshev and Fourier Spectram Methods. New York: Dover, 2001.

Chen, Shiyi, Darryl Holm, Len Margolin and Raoyang Zhang. ``Direct Numerical Simulations of the Navier-Stokes Alpha Model." Physica D. 133 (1999): 66–83.

Cheskidov, Alexey, Darryl Holm, Eric Olson and Edriss Titi. "On Leray-α model of turbulence." Proceedings of the Royal Society A: Mathematical, Physical and Engineering Sciences. 461 (2005): 629–649.

Holm, Darryl, Jerold Marsden and Tudor Ratiu. ``Euler-Poincaré Models of Ideal Fluids With Nonlinear Dispersion." Physical Review Letters. 349 (1998): 4173–4177.

Hou, Thomas, John Lowengrub and Michael Shelley. "Removing Stiffness from Interfacial Flows with Surface Tension." Journal of Computational Physics. 114(1994): 312–338.

Ilyin, A.A., E.M. Lunasin and E.S. Titi. "A Modified-Leray-Alpha Subgrid Scale Model of Turbulence." Nonlinearity. 19 (2006): 879–897.

Iserles, Arieh. A First Course in the Numerical Analysis of Differential Equations. New York: Cambridge University Press, 1996.

Kifowit, Steve. Fast Fourier Transforms. 8 Jan. 2005 <http://faculty.prairiestate.edu/skifowit/fft>.

Knobel, Roger. "An Introduction to Mathematical Theory of Waves." Student Mathematical Library (STML)/IAS/Park City Mathematical Subseries 3 (1999).

Krasny, Robert. "A study of singularity formation in a vortex sheet by the point vortex method." Journal of Fluid Mechanics. 65 (1986): 167.

Leray, Jean. "Sur les movements d'un fluide visqueux remplaissant l'espace." Acta Mathematica 63(1934): 193.

LeVeque, Randall. Numerical Methods for Conservation Laws. Basel: Birkhauser Verlag, 1992.

Linshiz, Jasmine and Edriss Titi. Analytical Study of Certain Magnetohydrodynamic-α Models. Eprintweb. June 1996. <http://arxiv.org/pdf/math/0606603>

Strauss, Walter. Partial Differential Equations. John Whiley and Sons, 1992.

Strikwerda, John. Finite Difference Schemes and Partial Differential Equations. Philadelphia:SIAM, 2004.

Tadmor, Etan. "Burgers Equation with Vanishing Hyper-Viscosity." Communications in Mathematical Sciences. 2(2004): 317–324

Tadmore, Etan, Edriss Titi and Weigang Zhong. "A Vanishing Leray-α Model of Burgers Equation." (in preparation)

Thomas, James. Numerical Partial Differential Equations. New York: Springer-Verlag, 1995.